HOKKAIDO UNIVERSITY

Title	Quantum-Confined Stark Effect Analysis of GeSn/SiGeSn Quantum Wells for Mid-Infrared Si-Based Electroabsorption Devices Based on Many-Body Theory
Author(s)	Fujisawa, Takeshi; Saitoh, Kunimasa
Citation	IEEE journal of quantum electronics, 51(11), 8400207 https://doi.org/10.1109/JQE.2015.2488363
Issue Date	2015-11
Doc URL	https://hdl.handle.net/2115/60344
Rights	©2015 IEEE. Personal use of this material is permitted. Permission from IEEE must be obtained for all other uses, in any current or future media, including reprinting/republishing this material for advertising or promotional purposes, creating new collective works, for resale or redistribution to servers or lists, or reuse of any copyrighted component of this work in other works.
Type	journal article
File Information	ujisawa-JQE-final.pdf

Hokkaido University Collection of Scholarly and Academic Papers : HUSCAP

Quantum-Confined Stark Effect Analysis of GeSn/SiGeSn Quantum wells for Mid-Infrared Si-Based Electroabsorption Devices Based on Many-Body Theory

T. Fujisawa, *Member IEEE*, and K. Saitoh, *Member IEEE*

***Abstract*— Quantum-confined Stark effect (QCSE) of group IV Ge(Sn)/SiGe(Sn) quantum wells (QWs) on Si substrate is analyzed by microscopic many-body theory for mid-infrared Si-based electroabsorption devices. To show the validity of the theory, QCSE of Ge/SiGe QW is investigated and very good agreement between theory and reported measured results is obtained. Next, QCSE of GeSn/SiGeSn QWs is analyzed and the QW design for electroabsorption modulators to obtain large extinction ratio in mid-infrared region is presented. It is shown that compressive and tensile strained well and barrier layers is preferable to obtain large extinction ratio due to its large conduction band offset.**

***Index Terms* — Si photonics, GeSn quantum wells, electroabsorption modulators, quantum-confined Stark effect, and many-body theory.**

I. Introduction

Optical devices for mid-infrared (mid-IR) wavelength region (2 to 5 μm) have attracted great attention for an environmental gas sensing and new wavelength optical communication system using photonic bandgap fiber and this research field is called "mid-IR photonics" [1]. Along with optical devices using conventional III-V material [2], Si-based mid-IR devices are also intensively studied since they can be fabricated in a CMOS environment, leading to lower cost of devices. In [3], some passive components using Si waveguides such as arrayed waveguide grating and concave grating, GeSn photo-diodes, and hybridly integrated GaSb light sources fabricated on Si substrate were demonstrated. Among them, light sources are crucial components for both sensing and communication applications. For light sources that can be monolithically integrated with other components on Si substrate, GeSn is one of the promising material. By introducing small amount of Sn into Ge, it is known that the bandgap (of GeSn) is drastically reduced and reaches mid-IR region [4]. Also, GeSn with Sn fraction exceeds about 10%, the Γ–bandgap becomes smaller than that of L-bandgap, and GeSn becomes direct bandgap material. Direct transition photoluminescence and p-doping were experimentally observed and realized on GeSn buffer layer grown on Si substrate [5]. Therefore, GeSn is a promising material for Si-based mid-IR light sources.

Recently, the first GeSn laser was successfully demonstrated by using bulk GeSn and optical pumping [6]. Various designs of GeSn quantum wells (QWs) were also investigated for obtaining large material gain and differential gain [7,8].

Other important active component is an electroabrsorption (EA) device. EA devices can be used for various optical signal processing, such as switching, and one of the most important application is an EA modulator (EAM) due to its high-speed characteristics [9,10]. EAMs and lasers can be (in principle) monolithically integrated, and therefore, an on-chip optical communication may be possible by integrating all the components (lasers, modulators, and detectors) on the same Si chip by using mid-IR wavelengths.

Recently, strong EA based on quantum-confined Stark effect (QCSE) was observed in Ge/SiGe QWs on Si substrate around 1.45 μm [11]. By incorporating small amount of Sn into the well, it can be used as mid-IR EAM. However, the QCSE of group IV QWs in mid-IR region has not been investigated so far.

In this paper, the QCSE of group IV QWs, Ge(Sn)/SiGe(Sn), is investigated by using microscopic many-body theory (MBT) [8,12-16]. MBT does not need any fitting parameters used in conventional analysis method to obtain optical properties of QWs, except for the effect of inhomogeneous broadening [13] originating from fabrication imperfection. First, the QCSE of Ge/SiGe QWs [11] is analyzed and the results show that calculated absorption spectra are in very good agreement with the experiment, showing the validity of MBT. It should be noted that this is the first time that MBT is applied to the analysis of QCSE of group IV QWs. Next, the effect of Sn-incorporation is investigated for mid-IR EAM applications. It is shown that QWs with compressively strained well and tensile strained barrier is effective to obtain large contrast between ON and OFF states.

II. Analysis Methods

A. Band structure and absorption spectrum

Figure 1 shows the QW structure analyzed here. (Si)Ge(Sn) buffer is placed on Si substrate and QW structures are grown on the buffer layer. The well is Ge(Sn) and the barrier is SiGe(Sn)

Manuscript received October 9, 2015. Authors are with the Graduate school of information science ant technologies, Hokkaido University, North 14 West 9, Sapporo, Hokkaido, 060-0814 Japan (e-mail: fujisawa@ist.hokudai.ac.jp).

and their thickness and strain are L_w and ε_w, L_B and ε_B. The band structure of QWs is calculated by $\boldsymbol{k \cdot p}$ theory [8,14]. To treat QCSE, the effect of applied electric field, F, is taken into account. We assume that the bias electric field is effective only in the well region and the band offset is constant under the electric field.

By solving $\boldsymbol{k \cdot p}$ equation, we obtain subband energies of the conduction, heavy-hole, light-hole, and split-off bands together with their wavefunctions for given transverse wavenumber and F. From the wavefunctions, the dipole matrix element for the transition between conduction and valence subbands is obtained by calculating the overlap of the two wavefunctions. These subband energies and matrix elements are the input for calculating the material absorption by MBT as explained in the following.

For the absorption spectra of QWs, although conventional free-carrier theory (FCT) based on Fermi's golden rule gives a simple explicit formula, it is well-known that the magnitude and position of absorption spectra are not consistent with the experiment [12-14]. For EAM design, in addition to the magnitude, the position of absorption spectra is also very important since the detuning from the lasing wavelength largely affects the total device performance. Also, the inclusion of exciton effect is important to properly calculate the bandedge absorption. Although in FCT, one needs extra treatment to include exciton effect [17], it is naturally incorporated in the framework of MBT. Therefore, we used microscopic MBT for the calculation of absorption spectra. By formulating the problem on the basis of second quantization, the so-called semiconductor Bloch equation can be derived

$$\frac{dp_{k_t}}{dt} = -i\omega_{k_t} p_{k_t} - i\Omega_{k_t}\left(f_e + f_h - 1\right) + \left.\frac{\partial p_{k_t}}{\partial t}\right|_{col} \qquad (1)$$

where k_t is the transverse wavenumber parallel to the QW plane, p_{kt} is the microscopic polarization, $\hbar\omega_{kt}$ is the renormalized transition energy, and Ω_{kt} contains the interaction term between the light and the carrier. f_e and f_h are Fermi-Dirac distributions for electrons and holes. The final term in (1) is the scattering contribution and derived from the commutation of Hamiltonian and the operator for p_{kt}. The detailed formulation and numerical treatment can be found in [8,12,18].

By discretizing (1) for the steady-state condition (the left-hand side of (1) is zero), we obtain a simultaneous equation and by solving it, the microscopic polarization is calculated for discretized k_t and a macroscopic polarization, P_{macro}, is obtained by summing the microscopic polarization over all the states. The macroscopic polarization is related to material absorption through Maxwell's equations as

$$\alpha(\hbar\omega) = -\mathrm{Im}\left[\frac{P_{macro}}{\varepsilon_0 n_B^2 E_0}\right] = -\mathrm{Im}\left[\frac{2}{\varepsilon_0 n_B^2 E_0 V}\sum_{k_t}\mu_{k_t}^{*} p_{k_t}\right] \qquad (2)$$

where ε_0 is the permittivity in vacuum, n_B is the background refractive index, V is the volume, μ_{kt} is the dipole matrix element, and E_0 is the electric field of light. The theory enables us to account for various important physical phenomena, such as the absorption peak due to excitons, bandgap renormalization, and the collapse of the absorption peak due to Coulomb screening effects, which cannot be considered in FCT.

Here, the absorption between L- conduction and valence bands is neglected due to the small absorption, especially at the band edge, originating from momentum mismatch [19]. As shown later, the experimental results are in good agreement with the calculated ones, showing the validity of the assumption.

Room temperature (298K) is assumed for all the results.

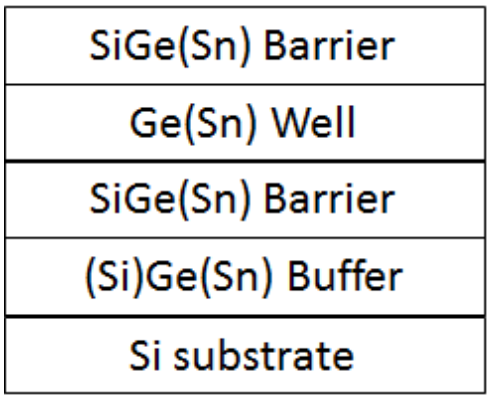


Fig. 1. Layer structure.

TABLE1. Band parameters of Si, Ge and Sn.

Parameters	Si	Ge	Sn
Lattice constant a [nm]	0.5430	0.5657	0.6489
Effective mass of Γ-conduction band m_c ($/m_0$)	0.156[21]	0.041[21]	0.058
Luttinger parameters			
γ_1	4.285	13.38	-14.97
γ_2	0.339	4.28	-10.61
γ_3	1.446	5.68	-8.52
Average valence band energy $E_{v,ave}$ [eV]	-0.48	0	0.64
Bandgap E_g [eV]	4.185	0.8	-0.413
Spin-orbit splitting energy Δ [eV]	0.044	0.29	0.8
Hydrostatic deformation potentials			
a_c [eV]	-10.39[20]	-8.24[20]	-6
a_v [eV]	1.8[20]	1.24[20]	1.58
Shear deformation potential b [eV]	-2.1[20]	-2.9[20]	-2.26
Elastic constants			
C_{11} [$\times 10^{10}$ N/m^2]	16.577	12.853	6.9
C_{12} [$\times 10^{10}$ N/m^2]	6.393	4.82	2.93
Bulk matrix element E_p [eV]	26.92[20]	25.49[20]	24

m_0 : electron mass in vaccum
If the reference number is not added, the value is taken from [7].

B. *Band parameters of SiGeSn*

The basic band parameters of Ge, Si, and Sn are taken from [7,20-26]. The bandgap of $Si_xGe_ySn_z$ alloy is given by

$$E_{g,SiGeSn}(x,y) = xE_{g,Si} + yE_{g,Ge} + zE_{g,Sn} - xyb_{SiGe} - zxb_{SiSn} - yzb_{GeSn} \qquad (3)$$

where $z = 1\text{-}x\text{-}y$. $E_{g,Si}$, $E_{g,Ge}$, and $E_{g,Sn}$ are the bulk bandgap of Si, Ge, and Sn. $b_{SiGe} = 0.21$ eV, $b_{GeSn} = 1.94$ eV, and $b_{SiSn} = 13.2$ eV are bowing parameters. Other band parameters are given by simple linear interpolations, namely,

$$P_{SiGeSn}(x,y) = xP_{Si} + yP_{Ge} + zP_{Sn} \qquad (4)$$

where P is the band parameters of interest (lattice constant, Luttinger parameters, etc) and they are summarized in Table I.

The band lineup of QWs is determined by model-solid theory [27]. The top of valence band of the alloy is given by

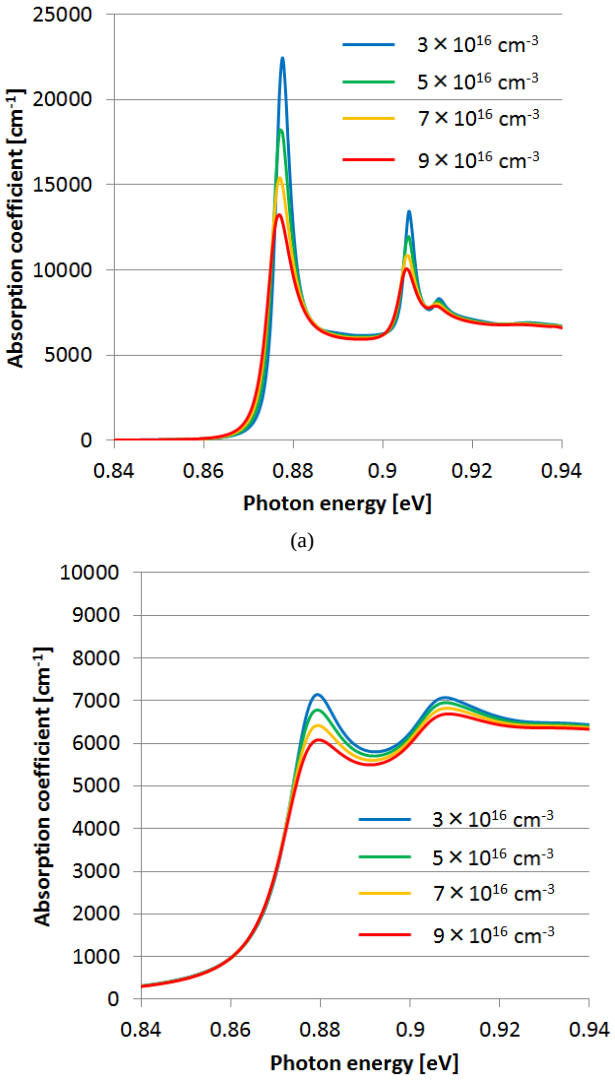


Fig. 2. Calculated absorption spectra of Ge/SiGe QWs for various carrier densities (a) without and (b) with Lorentzian broadening of 7.5 meV broadening energy.

$$E_{v,top} = E_{v,ave} + \frac{\Delta}{3} \tag{5}$$

III. QCSE OF GE/SIGE QUANTUM WELLS

Here, we consider Ge/SiGe QW on SiGe buffer on Si substrate [11] to show the validity of MBT. L_w and ε_w are 10 nm and -0.2%. L_B and ε_B are 20 nm and 0.4%. The minus sign for the strain means compressive strain. Although the experimental composition and the thickness of the buffer layer is $Si_{0.9}Ge_{0.1}$ and 500 nm, it was pointed out in [19] that the tensile strain posed by Si substrate cannot be fully relaxed. To take into account this correction, we use $Si_{0.95}Ge_{0.05}$ buffer [19] in our simulation.

Figure 2 (a) shows the absorption spectra of Ge/SiGe QWs obtained by MBT for the carrier density from 3 to 9×10^{16} cm^{-3} (low carrier density region). For low carrier density, the exciton absorption peak is very sharp and it is rapidly collapsed for large carrier density due to Coulomb screening effect.

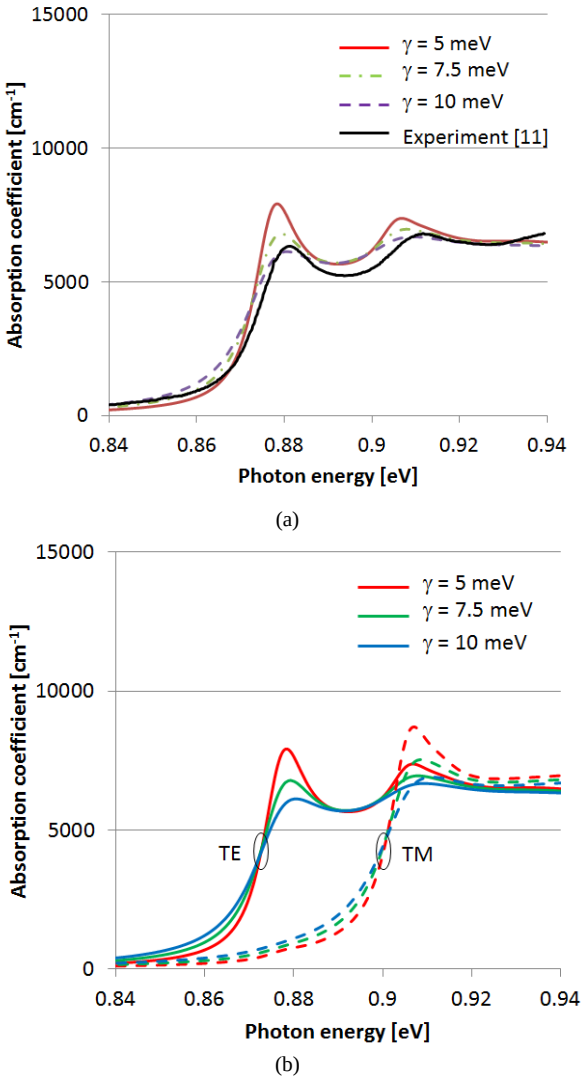


Fig. 3. (a) TE mode absorption spectra of Ge/SiGe QW without bias electric fields. The measured data are taken from [11]. (b) TE and TM mode absorption spectra of Ge/SiGe QW without bias electric fields.

Since there is always "inhomogeneous broadening" in the experimental optical spectra originating from, for example, a fabrication imperfection, we take into account the effect by following equation.

$$\alpha_{broaden}(\hbar\omega_0) = \int d\omega \alpha_{MBT}(\hbar\omega) L(\hbar\omega_0 - \hbar\omega) \tag{6}$$

where α_{MBT} is the absorption coefficient calculated by MBT. L is called broadening function and various types of functions have been proposed. Here, we use Lorentzian function given by

$$L(\hbar\omega_0 - \hbar\omega) = \frac{1}{\pi\gamma} \frac{\gamma^2}{\gamma^2 + (\hbar\omega_0 - \hbar\omega)^2} \tag{7}$$

where γ is the broadening energy.

Figure 2 (b) shows the same absorption spectra shown in Fig. 2 (a) but with Lorentzian broadening of γ = 7.5 meV. The sharp exciton peak almost vanishes and carrier density dependence of the spectra becomes very small. Figure 3 (a) shows the calculated absorption spectra without electric field for different γ values, at the carrier density of 5×10^{16} cm^{-3}. Measured spectrum at 0 V is also plotted (taken from [11]). Calculated and

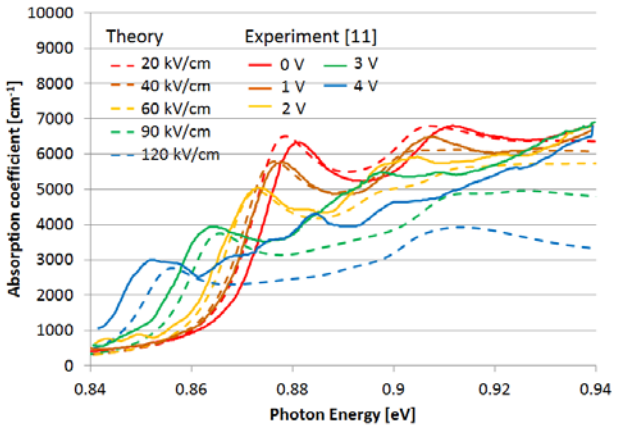


Fig. 4. Voltage dependent absorption spectra of Ge/SiGe QW. The measured data are taken from [11].

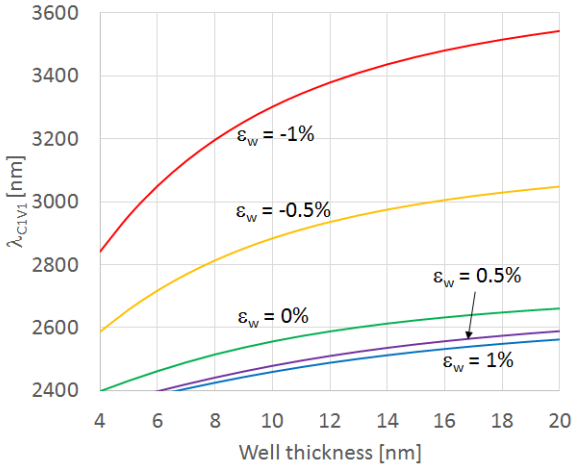


Fig. 5. C1V1 wavelength of GeSn QW as a function of well thickness for various values of well strain.

measured results are in very good agreement, and therefore, we use Lorentzian broadening with γ = 7.5 meV and the carrier density of 5×10^{16} cm^{-3} for the theoretical results hereafter.

Figure 3 (b) shows the absorption spectra of Ge/SiGe QW for both TE (solid) and TM (dashed) polarizations. Since the well has large compressive strain, the first and second valence subbands are heavy- and light-hole bands. Therefore, the photon energy of the absorption edge for TM mode is larger than that of TE mode.

Solid and dashed lines in Fig. 4 show measured [11] and calculated absorption spectra of Ge/SiGe QW for different values of voltage and electric field. According to [11], total thickness of the intrinsic layer is 576 nm, and the electric field corresponding to experimental 1 V is about 20 kV/cm. The built-in electric field is also about 20 kV/cm [19]. From the figure, excellent agreement between theory and experiment can be seen for 0, 1, and 2 V in terms of spectral position and shape including exciton absorption peak, showing the validity of MBT used here. For 3 and 4 V, although the theoretical electric field matching to the position of experimental spectra is larger than expected, the bandedge spectral position and shape are well reproduced. The discrepancy between the theoretical electric field and experimental voltage may come from unintentional background doping in the intrinsic region. Background doping results in non-uniform applied electric field for multiple quantum well structure even with very small doping level of 10^{15} cm^{-3} [28]. Also, especially for 3 and 4 V, although the bulk absorption increase for larger photon energy can be seen for experimental spectra, it is not taken into account in our simulation.

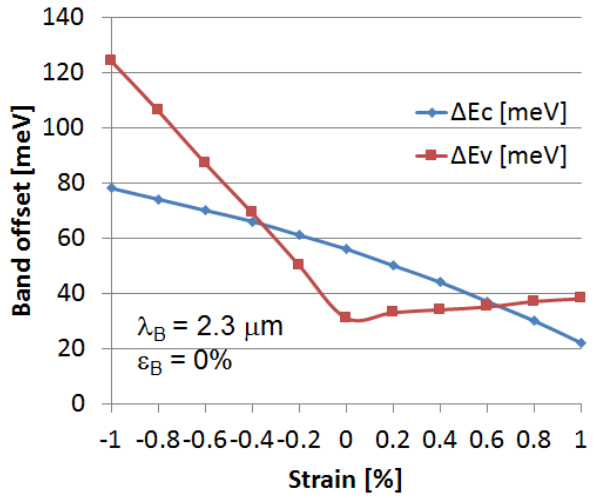
IV. QCSE of GeSn/SiGeSn Quantum Wells

In this section, the QCSE of GeSn/SiGeSn QWs on GeSn buffer is investigated for mid-IR EAM based on Si photonics. The buffer layer is assumed to be $Ge_{0.88}Sn_{0.12}$ whose bulk band structure has direct band gap [5]. Figure 5 shows the bandgap wavelength between first Γ conduction subband and first valence subband (C1V1 wavelength, λ_{C1V1}) of GeSn QW as a function of the well thickness and the strain. The barrier layer is assumed to be lattice matched to the buffer layer and the bandgap wavelength of the barrier layer is λ_B = 2.1 μm. Since SiGeSn has three elements, the composition is fully determined by its strain and bulk bandgap. Therefore, we specify the composition of SiGeSn by its strain and bulk bandgap instead of the composition. λ_{C1V1} ranges from 2.3 to 3.4 μm and useful for mid-IR applications. To enhance the QCSE, it is important to use deep well (large band offset), especially for conduction band. A deep well makes the confinement of electron and hole stronger, leading to larger absorption even when the electric field is applied [15]. Therefore, to design the GeSn/SiGeSn QWs for EAM, the QW structure having large band offset has to be investigated first to use QCSE effectively. And then, absorption and extinction characteristics are discussed based on the results of MBT.

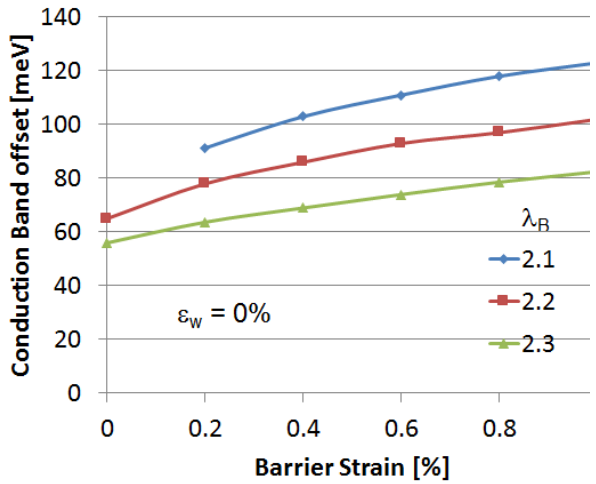
Figure 6 (a) shows the conduction band offset, ΔE_c, and the valence band offset, ΔE_v, as a function of ε_w. The bulk bandgap and the strain of the barrier layer are λ_B = 2.3 μm and ε_B = 0%. For the well, although compressive strain is better to obtain large ΔE_c, ΔE_v is also increased. Figure 6 (b) shows ΔE_c as a function of ε_B for different values of λ_B. The strain of the well layer is set to zero. From the Figure, we can see that tensile strain and small λ_B for the barrier layer make ΔE_c larger. Therefore, to obtain large ΔE_c, compressive and tensile strained well and barrier layers are preferable to obtain large extinction ratio.

Figure 7 (a) shows wavefunctions of the first conduction subbands for F = 0, 50, 100 kV/cm of GeSn/SiGeSn QW for L_w = 10nm, ε_w = 0%, ε_B = 0%, and λ_B = 2.3 μm (ΔE_c = 56 meV). Under large electric field, the wavefunction leaks to the barrier layer, leading to smaller overlap with valence band wavefunctions. Figure 7 (b) shows the same wavefunctions of QWs but with ε_w = -1% (ΔE_c = 78 meV). Due to the stronger confinement of electrons in the well, the leak to the barrier layer is suppressed and overlap between conduction and valence wavefunctions becomes large, leading to larger contrast between ON and OFF states of EAM.

Figures 8 (a), (b), and (c) show absorption spectra of

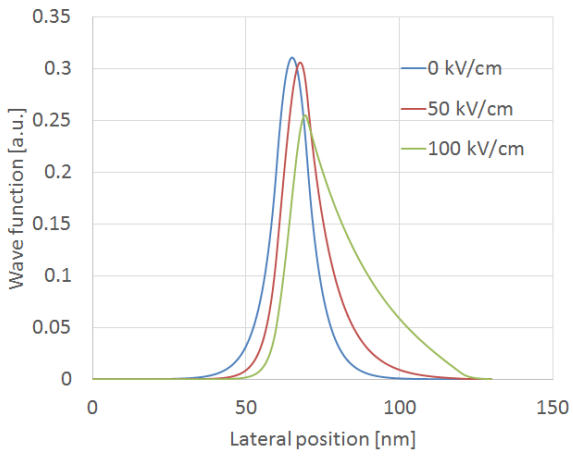


(a)

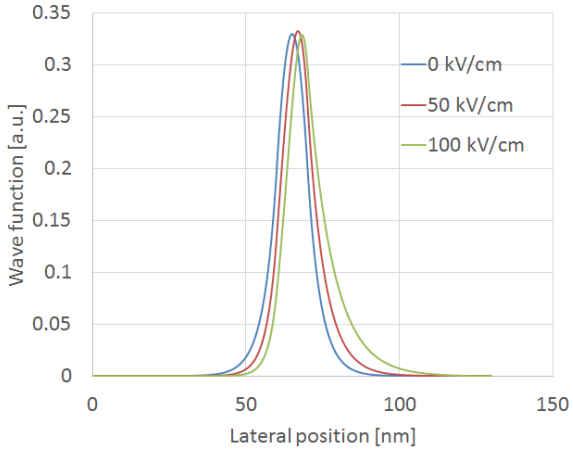


(b)

Fig. 6. (a) ΔE_c and ΔE_v of GeSn/SiGeSn QW as a function of ε_w. The barrier wavelength and strain are 2.3 μm and 0%. (b) ΔE_c of GeSn/SiGeSn QW as a function of ε_B. The well strain is 0%.



(a)



(b)

Fig. 7. Wavefunctions of the first conduction subband for different bias electric fields of GeSn/SiGeSn QWs for (a) ε_w = 0%, ε_B = 0%, and λ_B = 2.3 μm and (b) ε_w = -1%, ε_B = 0%, and λ_B = 2.3 μm.

GeSn/SiGeSn QWs. The structural parameters for each Figure are (a) ε_w = 0%, ε_B = 0%, λ_B = 2.2 μm, ΔE_c = 72 meV, ΔE_c = 46 meV, (b) ε_w = -0.4%, ε_B = 0.2%, λ_B = 2.1 μm, ΔE_c = 100 meV, ΔE_c = 103 meV, and (c) ε_w = -1%, ε_B = 0.5%, λ_B = 2.1 μm, ΔE_c = 130 meV, ΔE_c = 171 meV. L_w = 10 nm. Although the broadening parameter for Sn-based alloy is not known well, we use the same parameters as in Ge/SiGe QW (Lorentzian broadening with γ = 7.5 meV). ε_B is determined by strain compensation condition given by

$$\frac{\varepsilon_w L_w + \varepsilon_B L_B}{L_w + L_B} = 0 \tag{8}$$

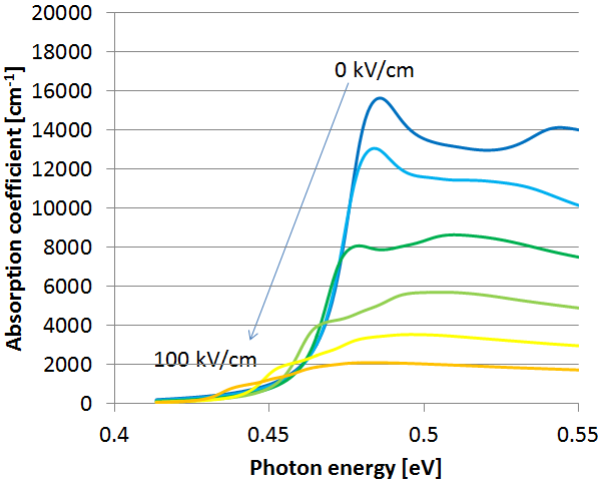
The absorption spectra are plotted from 0 kV/cm with 20 kV/cm interval. For lattice matched QW (Fig. 4 (a)), the bandedge absorption change is so small due to small ΔE_c that the structure is not suitable for EAM application. For larger compressive strain in the well, clear QCSE red-shift can be seen for larger values of electric fields. The magnitude of absorption coefficient is larger for larger values of compressive strain in the well. Therefore, large compressive strained well and tensile strained barrier is effective to enhance the absorption under the electric field, resulting in EAMs with large extinction ratio.

Next, we discuss the extinction ratio (ER) of GeSn/SiGeSn EAMs. We consider silica ridge structure proposed in [7] with the optical confinement factor of 7%, which is reasonable value for most multiple QW waveguides. The length of the waveguide is set to 200 μm, which is typical value for high-speed EAMs. The ER is calculated by

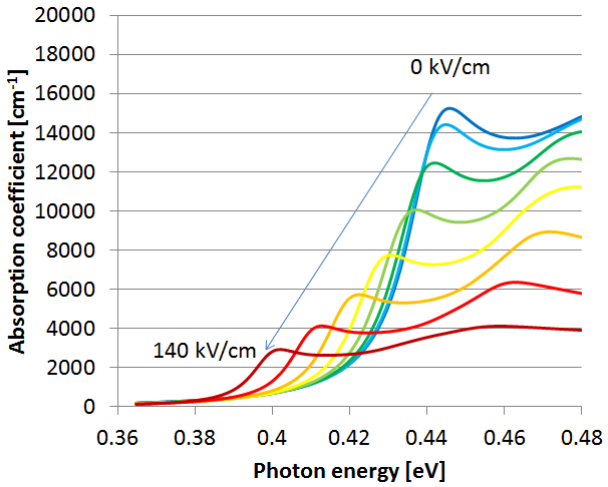
$$ER = 10\log_{10}\left[-\Gamma \alpha_{broaden}(\hbar\omega_0, F) L_{EA}\right] \tag{9}$$

where Γ is the optical confinement factor, λ is the incident wavelength, L_{EA} is the length of EAMs. Figure 9 shows the ER of GeSn/SiGeSn QW waveguide. The QW structural parameters for blue and red lines are identical to those of Fig. 8 (b) and (c). The incident wavelengths for blue and red lines are 3.1 and 3.625 μm (0.4 and 0.342 eV). Static ERs of more than 10 and 20 dB can be obtained for the structures.

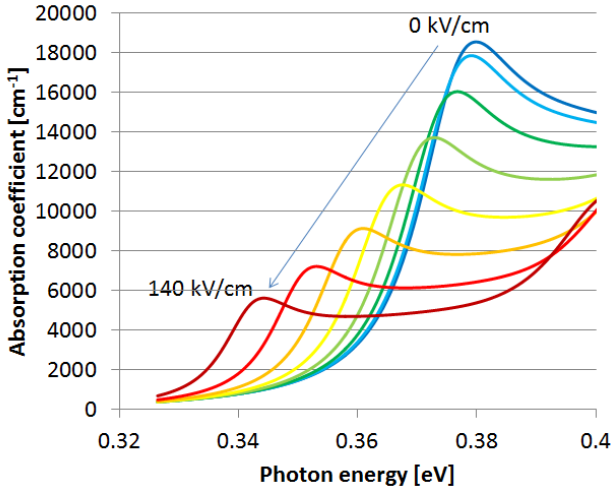
For modulator applications, the depth of the well, especially for the valence band, affects the high-speed characteristics due to the hole-pile-up effect. Therefore, not only ΔE_c but also the valence band offset, ΔE_v, is important for the EAM design. As shown in Fig. 6 (a), for GeSn/SiGeSn QWs, if the value of ε_w is



(a)



(b)



(c)

Fig. 8. Absorption spectra of GeSn/SiGeSn QWs. The structural parameters are (a) ε_w = 0%, ε_B = 0%, λ_B = 2.2 μm, ΔE_c = 72 meV, ΔE_c = 46 meV, (b) ε_w = -0.4%, ε_B = 0.2%, λ_B = 2.1 μm, ΔE_c = 100 meV, ΔE_c = 103 meV, and (c) ε_w = -1%, ε_B = 0.5%, λ_B = 2.1 μm, ΔE_c = 130 meV, ΔE_c = 171 meV.

large, both the conduction and valence band offsets become large. Therefore, there is a tradeoff between available extinction ratio and high-speed characteristics. Since the state of the art

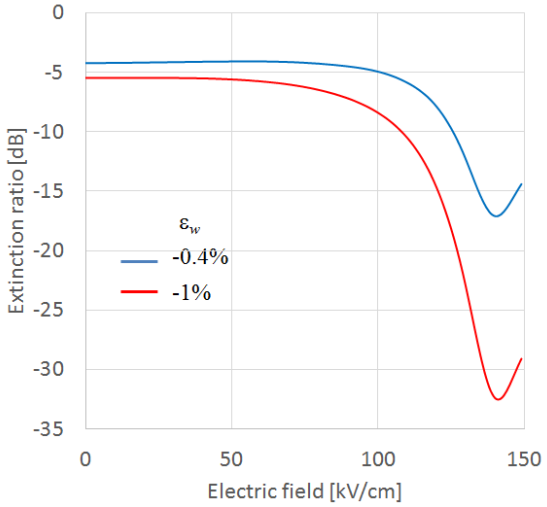


Fig. 9. ER of GeSn/SiGeSn waveguides as a function of bias electric fields. The structural parameters for blue and red lines are identical to those of Fig. 8 (b) and (c). The incident wavelengths for blue and red lines are 3.1 and 3.625 μm.

40-Gbit/s EAM for 1.55 μm using InAlGaAs-based QWs employ the valence band offset around 120 meV [29], similar valence band offset is available for GeSn/SiGeSn QWs.

CONCLUSION

We have investigated QCSE of group IV QWs by using MBT. For Ge/SiGe QW, calculated and measure results are in very good agreement, showing the validity of MBT for the QCSE analysis of group IV QWs. The QCSE analysis of GeSn/SiGeSn QWs were also performed for mid-IR Si-based EAM. To enhance the absorption under the electric field, and hence, large extinction ratio, it was found that the strain compensation structure (compressive strained well and tensile strained barrier) with large strain is useful due to the large ΔE_c.

REFERENCES

[1] R. Soref, "Mid-infrared photonics in silicon and germanium," Nature Photon., vol.4, pp.495-497, Aug. 2010.

[2] B. Corbett, M. R. Gleeson, N. Ye, C. Robert, H. Yang, H. Zhang, N. Mac Suibhne, P. E.Morrissey, K. Thomas, A. Gocalinska, E. Pelucchi, R. Phelan, B. Kelly, J. O'Carroll, F. H. Peters and F.C. Garcia Gunning, "InP based active and passive components for communication systems at 2 μm," in Proc. ECOC2014, Tu.4.4.5, 2014.

[3] G. Roelkens, U.D. Dave, A. Gassenq, N. Hattasan, C. Hu, B. Kuyken, F. Leo, A. Malik, M. Muneeb, E. Ryckeboer, D. Sanchez, S. Uvin, R. Wang, Z. Hens, R. Baets, Y. Shimura, F. Gencarelli, B. Vincent, R. Loo, J.V. Campenhout, L. Cerutti, J.-B. Rodriguez, E. Tourni´e, X. Chen, M. Nedeljkovic, G. Mashanovich, Li Shen, N. Healy, A.C. Peacock, X. Liu, R. Osgood, and William M. J. Green, "Silicon-based photonic integration beyond the telecommunication wavelength range," *IEEE J. Sel. Top. Quantum Electron.*, vol. 20, pp.8201511, July 2014.

[4] G. Grzybowski, R. T. Beeler, L. Jiang, D. J. Smith, J. Kouvetakis, and J. Menéndez, "Next generation of $Ge_{1-y}Sn_y$ (y=0.01-0.09) alloys grown on Si(100) via Ge_3H_8 and SnD_4: Reaction kinetics and tunable emission", *Appl. Phys. Lett.*, vol. 101, pp. 072105, Aug. 2012.

[5] J. Mathews, R. T. Beeler, J. Tolle, C. Xu, R. Roucka, J. Kouvetakis, and J. Menéndez, "Direct-gap photoluminescence with tunable emission wavelength in $Ge_{1-y}Sn_y$ alloys on silicon," *Appl. Phys. Lett.*, vol. 97, pp. 221912, Nov. 2010.

[6] S. Wirths, R. Geiger, N. Von den Driesch, G. Mussler, T. Stoica, S.. Mantl, Z. Ikonic, M. Luysberg, S. Chiussi, J.M. Hartmann, H. Sigg, J.

Faist, D. Buca, and D. Grutzmacher, "Lasing in direct-bandgap GeSn alloy grown on Si," Nature Photon., vol.9, pp.88-92, Feb. 2015.

[7] G.-E. Chang, S.-W. Chang, and S.L. Chuang, "Strain-balanced Ge_zSn_{1-z}-$Si_xGe_ySn_{1-x-y}$ multiple-quantum-well lasers," *IEEE J. Quantum Electron.*, vol. 46, pp.1813-1820, Dec. 2010.

[8] T. Fujisawa and K. Saitoh, "Material gain analysis of GeSn/SiGeSn quantum wells for mid-infrared Si-based light sources based on many-body theory," *IEEE J. Quantum Electron.*, vol.51, pp.7100108, May 2015.

[9] T. Fujisawa, K. Takahata, W. Kobayashi, T. Tadokoro, N. Fujiwara, S. Kanazawa, and F. Kano, "1.3-μm, 50-Gbit/s electroabsorption modulators integrated with a DFB laser for beyond 100G parallel LAN applications," *IET Electron. Lett*., vol. 47, pp.709-710, June 2011.

[10] T. Fujisawa, S. Kanazawa, K. Takahata, W. Kobayashi, T. Tadokoro, H. Ishii, and F. Kano, "1.3-μm, 4×25G, EADFB laser array module with large-output-power and low-driving-voltage for energy-efficient 100GbE transmitter," *Optics Express*, vol.20, pp.614-620, Jan. 2012.

[11] Y.H Kuo, Y.K. Lee, Y. Ge, S. Ren, J.E. Roth, T.I. Kamins, D.A.B. Miller, and J.S. Harris, "Strong quantum-confined Stark effect in germanium quantum-well structures on silicon," *Nature*, vol. 437, pp.1334-1336, Oct. 2005.

[12] W.W. Chow and S.W. Koch, "Semiconductor-laser fundamentals," Springer, 1993.

[13] J. Hoder, J.V. Moloney, and S.W. Koch, "Microscopic evaluation of spontaneous emission and Auger processes in semiconductor lasers," *IEEE J. Quantum Electron*., vol. 41, pp.1217-1226, Oct. 2005.

[14] T. Fujisawa, T. Sato, M. Mitsuhara, T. Kakitsuka, T. Yamanaka, Y. Kondo, and F. Kano, "Successful application of the 8-band $\boldsymbol{k \cdot p}$ theory to optical properties of highly strained In(Ga)As/InGaAs quantum wells with strong conduction-valence band coupling," *IEEE J. Quantum Electron.*, vol. 45, pp.1183-1191, Sep. 2009.

[15] T. Fujisawa, M. Arai, and F. Kano, "Many-body design of highly strained GaInNAs electroabsorption modulators on GaInAs ternary substrates," *J. Appl. Phys*., vol. 107, pp. 093107, May 2010.

[16] T. Fujisawa, T. Yamanaka, T. Tadokoro, N. Fujiwara, M. Arai, W. Kobayashi, Y. Kawaguchi, K. Tsuzuki, and F. Kano, "Theoretical and experimental investigations of the incident-power-dependent extinction ratio of electroabsorption modulator integrated with DFB laser," *IEEE J. Quantum Electron*., vol. 47, pp.60-65, Jan. 2011.

[17] J.P. Loehr and J. Singh, "Nonvariational numerical calculations of excitonic properties in quantum wells in the presence of strain, electric fields, and free carriers," *Phys. Rev. B*, vol. 42, pp. 7154-7162, Oct. 1990.

[18] H. Haug and A.P. Jauho, "Quantum kinetics in transport and optics of semiconductors," Springer, 2008.

[19] J. Kim and D. Ahn, "Effect of indirect interband absorption in Ge/SiGe quantum wells," *J. Appl. Phys*., vol. 110, pp. 083119, Aug. 2011.

[20] D.J. Paul, "8-band k.p modeling of the quantum confined Stark effect in Ge quantum wells on Si substrates," *Phys. Rev. B*, vol. 77, pp. 155323, Apr. 2008.

[21] Y.H Kuo, Y.K. Lee, Y. Ge, S. Ren, J.E. Roth, T.I. Kamins, D.A.B. Miller, and J.S. Harris, "Quantum-confined Stark effect in Ge/SiGe quantum wells on Si for optical modulators," *IEEE J. Sel. Topics in Quantum Electron.*, vol. 12, pp.1503-1513, Nov./Dec. 2006.

[22] V. R. D'Costa, C. S. Cook, A. G. Birdwell, C. L. Littler, M. Canonico, S. Zollner, J. Kouvetakisand, and J. Menéndez, "Optical critical points of thin-film $Ge_{1-y}Sn_y$ alloys: A comparative $Ge_{1-y}Sn_y/Ge_{1-x}Si_x$ study," *Phys. Rev. B*, vol. 73, no. 12, pp. 125207–125222, Mar. 2006.

[23] P. Moontragoon, Z. Ikoni´c, and P. Harrison, "Band structure calculations of Si-Ge-Sn alloys: Achieving direct band gap materials," *Semicond. Sci. Technol.*, vol. 22, no. 7, pp. 742–748, 2007.

[24] V. R. D'Costa, Y.-Y. Fang, J. Tolle, J. Kouvetakis, and J. Menéndez, "Tunable optical gap at a fixed lattice constant in group-IV semiconductor alloys," *Phys. Rev. Lett.*, vol. 102, no. 10, pp. 107403–107406, 2009.

[25] J. Mathews, R. T. Beeler, J. Tolle, C. Xu, R. Roucka, J. Kouvetakis, and J. Menéndez, "Direct-gap photoluminescence with tunable emission wavelength in $Ge_{1-y}Sn_y$ alloys on silicon," *Appl. Phys. Lett*., vol.97, pp. 221912, Nov. 2010.

[26] Robert Chen, Hai Lin, Yijie Huo, Charles Hitzman, Theodore I. Kamins, and James S. Harris, "Increased photoluminescence of strain-reduced, high-Sn composition Ge1-xSnx alloys grown by molecular beam epitaxy," *Appl. Phys. Lett*., vol.97, pp. 181125, Oct. 2011.

[27] C. G. V. de Walle, "Band lineups and deformation potentials in the model-solid theory," *Phys. Rev. B*, vol. 39, pp. 1871–1883, Jan.1989.

[28] T. Arakawa, T. Hariki, Y. Amma, M. Fukuoka, M. Ushigome, and K. Tada, "Low-voltage Mach-Zhender modulator with InGaAs/InAlAs five-layer asymmetric coupled quantum well," *J. J. Appl. Phys*., vol. 51, pp. 042203, Apr. 2012.

[29] W. Kobayashi, M. Arai, T. Yamanaka, N. Fujiwara, T. Fujisawa, T. Tadokoro, K. Tsuzuki, Y. Kondo, and F. Kano, "Design and fabrication of 10-/40-Gbit/s, uncooled electroabsorption modulator integrated DFB laser with butt-joint structure," *J. Lightwave Technol.*, vol. 28, pp.164-171, Jan. 2010,



Takeshi Fujisawa (M'05) was born in Sapporo, Japan, on January 12, 1979.He received the B.E., M.E., and Ph.D. degrees in electronic engineering from Hokkaido University, Sapporo, in 2001, 2003, and 2005, respectively. He was a Research Fellow of the Japan Society for the Promotion of Science from 2003 to 2006. In 2006, he joined the Nippon Telegraph and Telephone (NTT) Photonics Laboratories, NTT Corporation, Atsugi, Japan. In 2014, he became an Associate Professor at the Graduate School of Information Science and Technology, Hokkaido University. His research interests include active optical devices for optical communication systems, such as semiconductor lasers and modulators, and theoretical modeling of optical fibers and devices. He is an author or coauthor of more than 50 papers in international refereed journals.

Prof. Fujisawa has been served as an Associate Editor of Optics Express from 2014 and is a Member of the Institute of Electronics, Information and Communication Engineers of Japan.



Kunimasa Saitoh (S'00–M'01) received the B.S., M.S., and Ph.D. degrees in electronic engineering from Hokkaido University, Sapporo, Japan, in 1997, 1999, and 2001, respectively. From 1999 to 2001, he was a Research Fellow of the Japan Society for the Promotion of Science. From 2001 to 2005, he was a Research Associate with the Graduate School of Engineering, Hokkaido University. From 2005 to 2013, he was an Associate Professor at Graduate School of Information Science and Technology, Hokkaido University, and in 2013, he became a Professor there. He has been involved in research on fiber optics, nano-photonics, integrated optical devices, and computer-aided design and modeling of guided-wave devices using finite element method, beam propagation method, and so on. He is an author or coauthor of more than 150 research papers in refereed international journals. Prof. Saitoh is a Member of the Optical Society of America, and the Institute of Electronics, Information and Communication Engineers. He received the Excellent Paper Award and the Young Scientist Award from the IEICE, in 1999 and 2002, respectively, the Young Scientists' Prize of the Commendation for Science and Technology from the Ministry of Education, Culture, Sports, Science, and Technology (MEXT), Government of Japan in 2008. From 2009 to 2010, he served as a Secretary/Treasurer of the IEEE Sapporo Section.